

WHERE ARE THE R-MODES? *CHANDRA* OBSERVATIONS OF MILLISECOND PULSARS

SIMIN MAHMOODIFAR AND TOD STROHMAYER

Astrophysics Science Division and Joint Space-Science Institute, NASA's Goddard Space Flight Center, Greenbelt, MD 20771, USA

Draft version October 9, 2018

Abstract

We present the results of *Chandra* observations of two non-accreting millisecond pulsars, PSRs J1640+2224 (J1640) and J1709+2313 (J1709), with low inferred magnetic fields and spin-down rates in order to constrain their surface temperatures, obtain limits on the amplitude of unstable r -modes in them, and make comparisons with similar limits obtained for a sample of accreting low-mass X-ray binary (LMXB) neutron stars. We detect both pulsars in the X-ray band for the first time. They are faint, with inferred soft X-ray fluxes (0.3 – 3 keV) of $\approx 6 \times 10^{-15}$ and 3×10^{-15} erg cm⁻² s⁻¹ for J1640 and J1709, respectively. Spectral analysis assuming hydrogen atmosphere emission gives global effective temperature upper limits (90% confidence) of $3.3 - 4.3 \times 10^5$ K for J1640 and $3.6 - 4.7 \times 10^5$ K for J1709, where the low end of the range corresponds to canonical neutron stars ($M = 1.4M_{\odot}$), and the upper end corresponds to higher-mass stars ($M = 2.21M_{\odot}$). Under the assumption that r -mode heating provides the thermal support, we obtain dimensionless r -mode amplitude upper limits of $3.2 - 4.8 \times 10^{-8}$ and $1.8 - 2.8 \times 10^{-7}$ for J1640 and J1709, respectively, where again the low end of the range corresponds to lower-mass, canonical neutron stars ($M = 1.4M_{\odot}$). These limits are about an order of magnitude lower than those we derived previously for a sample of LMXBs, except for the accreting millisecond X-ray pulsar (AMXP) SAX J1808.4–3658, which has a comparable amplitude limit to J1640 and J1709.

Subject headings: stars: neutron — stars: oscillations — X-rays: stars — Pulsars: individual (PSR J1640+2224 , PSR J1709+2313)

1. INTRODUCTION

Neutron stars (NSs) contain the densest matter in the universe outside of black holes, making them unique laboratories for the study of cold ultra-dense matter. Their cores may contain exotic forms of matter postulated to exist at supranuclear densities, including hyperons, strange quark matter, color superconducting quarks, and pion or kaon condensates. While constraints on the masses and radii of NSs are important for constraining the equation of state (EOS) of ultra-dense matter, observations of their dynamic properties, such as spin and thermal evolution, as well as their oscillation modes, are also important and could potentially be more efficient at discriminating between different phases of dense matter.

A key process that can affect the spin evolution of fast-rotating pulsars is the instability associated with the r -modes of neutron stars (Bildsten 1998; Andersson et al. 1999). These modes are axial pulsations in which the restoring force is the Coriolis force resulting from rotation of the star. The r -modes are unstable due to the emission of gravitational radiation. Since they are retrograde in the corotating frame of the star and appear prograde to a distant observer, they emit positive angular momentum in the form of gravitational waves, but since they have negative angular momentum in the corotating frame of the star, their amplitude grows due to emission of gravitational radiation. They may play a role in limiting the spin rates of neutron stars, since the gravitational radiation they emit carries away angular momentum and rotational kinetic energy. For example, it remains puzzling that the spin frequency distribution of Accreting Millisecond X-ray Pulsars (AMXPs) appears

to cut off well below the mass-shedding limit of essentially all realistic neutron star EOSs (Chakrabarty et al. 2003; Patruno 2010). White & Zhang (1997) suggested that magnetic braking could be responsible for halting the spin-up, while Bildsten (1998) proposed that it might be due to the emission of gravitational radiation, as could be produced, for example, by an unstable r -mode.

Whether or not the r -mode instability has a significant effect on the spin evolution of neutron stars strongly depends on the maximum amplitude to which they can grow. If their amplitudes are high enough they may be detectable by the new generation of gravitational wave detectors, such as advanced-LIGO, but even a small-amplitude r -mode can significantly limit the spin rate of a neutron star. The r -modes are unstable as long as their gravitational radiation timescale, τ_G , is less than their damping timescale, τ_{damp} . This competition leads to an instability window in the ν -T plane—where ν is the NS's spin frequency and T is its core temperature—given by a critical curve that is defined by $\tau_G = \tau_{damp}$. Interestingly, the instability window is sensitive to the phase of dense matter comprising the NS (Alford et al. 2012a).

In addition to braking the stars' rotation the r -modes also influence their thermal evolution by depositing heat into the star via the dissipation of pulsation energy. Both of these processes depend strongly on the r -mode amplitude. Several mechanisms to dampen the r -modes have been examined, including a viscous boundary layer at the core-crust interface (Bildsten & Ushomirsky 2000; Levin & Ushomirsky 2001), bulk viscosity enhanced by a hyperon-rich core (Haskell & Andersson 2010), supra-thermal bulk viscosity (Alford et al. 2010, 2012b), mu-

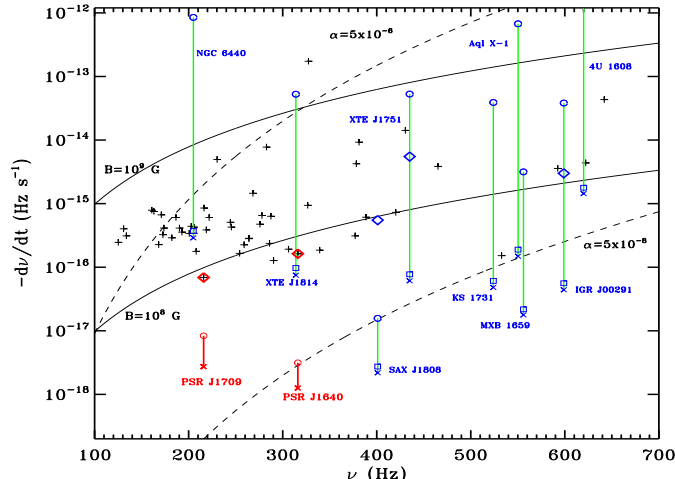


FIG. 1.— Limits on the spin-down rates due to an r -mode torque for nine LMXB systems (blue symbols and vertical green bars, adapted from MS13) and two non-accreting MSPs (red symbols and vertical bars, this work) are shown in the $\dot{\nu}$ vs. ν plane. The $\dot{\nu}$ limits for LMXB systems are shown for NS masses of 1.4 (\times symbols), 2.0 (square symbols), and 2.21 M_{\odot} (circle symbols). For LMXB systems with measured, quiescent spin-down rates, the values are marked with the blue diamonds. The r -mode spin-down limits derived for PSRs J1640 and J1709 for 1.4 (\times symbols) and 2.21 M_{\odot} (circle symbols) are shown in red. The observed spin-down rates for these pulsars are given by the red diamond symbols. For additional context, MSPs from the ATNF pulsar database are marked with the black + symbols (see MS13 for further details).

tual friction due to superfluid vortices (Haskell et al. 2009, 2014), mode coupling (Arras et al. 2003; Bondarescu et al. 2007, 2009), and magnetohydrodynamic effects (Rezzolla et al. 2000, 2001), but none of these has been shown to eliminate the r -mode instability and they leave the majority of fast-rotating NSs—such as the class of low-mass X-ray binaries (LMXBs)—inside the instability window for “standard” hadronic matter (Ho et al. 2011; Haskell et al. 2012; Alford & Schwenzer 2013; Mahmoodifar & Strohmayer 2013, hereafter MS13). The amplitude at which the r -mode growth will saturate, and thereby how much it can affect the spin and thermal evolution of NSs, is still unknown, but it is crucial for understanding the presence of fast-rotating NSs (such as the LMXBs) within the instability window. Thus, temperature and spin evolution measurements of these NSs can provide a unique probe of their r -mode amplitudes and physics, as well as its potential for constraining the interior properties of NSs.

In MS13 we determined upper limits on the amplitude of r -modes, and their gravitational-radiation-induced spin-down rates, in LMXB NSs under the assumption that the quiescent NS luminosity is powered by dissipation from a steady-state r -mode. We showed that upper limits on dimensionless r -mode amplitudes in LMXB NSs are in the range of 10^{-8} to 10^{-6} for lower mass (1.4 and 2.0 M_{\odot}) NS models and they are larger for high mass (2.21 M_{\odot}) models which support fast (direct Urca) neutrino emission in their cores. For the three AMXPs, a subset of the LMXBs, with known quiescent spin-down rates (marked with the blue diamond symbols in Fig. 1) these limits suggest that $\sim 1\%$ of the observed rate can be due to an r -mode. While there are currently only three robust spin-down measurements for AMXPs (Patruno & Watts 2012), spin-down rates are known for a much larger sample of millisecond pulsars (MSPs; shown by the black + symbols in Fig. 1), and some of these rates are comparable to the estimates of the r -mode spin-

down rates in low-mass NS models. This suggests the interesting possibility that gravitational radiation due to r -modes in these sources might have a significant contribution to their spin-down. If so, it may be that some of them have smaller magnetic fields than their values inferred from magnetic dipole spin-down alone. However, surface temperatures with which to constrain the r -mode amplitudes are presently not known for many of these pulsars. To date, only three MSPs have a global surface temperature estimate. These are the nearby MSPs, PSR J0437–4715 (Durant et al. 2012, hereafter J0437) and PSR J2124–3358 (Rangelov et al. 2017, hereafter J2124), with quite low surface temperature estimates of $\approx 1 - 4 \times 10^5$ K, and $0.5 - 2.1 \times 10^5$ K for J0437 and J2124, respectively. These estimates were derived from far UV HST observations. We note that J0437 is a slow spinner at 173.7 Hz and is likely outside the nominal instability window. Lastly, PSR J1231–1411 (Schwenzer et al. 2017, hereafter J1231) has an upper limit on the surface temperature of 1.7×10^5 K, that was obtained using *Chandra*, *XMM-Newton* and *SUZAKU* observations. Based on the discussion above we proposed to observe with *Chandra* a small number of MSPs with low spin-down rates but faster spin frequencies than J0437, in order to constrain their core temperatures and the effect of r -modes on their spin evolution. We obtained *Chandra* observations for two targets, PSRs J1640+2224 (hereafter, J1640) and J1709+2313 (hereafter, J1709), detecting both for the first time in the X-ray band. Both objects are long-period (see Table 1) neutron star binaries hosting low-mass white dwarf companions. Age estimates from white dwarf cooling indicate that the systems are very old, 5 - 7 Gyr (Desvignes et al. 2016; Löhmer et al. 2005; Lundgren et al. 1996). Their ages, combined with the long orbital periods, argues that these objects have likely not seen any significant accretion, that is, mass transfer due to Roche lobe overflow, in ≈ 100

Myr or longer (Willems & Kolb 2002). Such systems are therefore good laboratories for exploring NS heating processes, such as r -mode reheating. This paper is organized as follows. In section 2 we summarize the observations and data analysis. In section 3 we estimate the r -mode amplitude and spin-down rates in these sources. Finally, we provide some conclusions in section 4.

2. CHANDRA OBSERVATIONS AND DATA ANALYSIS

J1640 and J1709 were observed with the *Chandra X-ray Observatory* Advanced CCD Imaging Spectrometer (ACIS-S). The observation IDs, dates, exposures, and parameters relevant for our spectral analysis for each of these sources are presented in Table 1. We note that neither of these sources had a prior detection with either *Chandra*, *XMM-Newton*, *Swift* or indeed *ROSAT*.

In the following subsections we present our data analysis and methods for constraining the global surface temperature of these pulsars. We note that some MSPs show a soft X-ray thermal emission component that is very likely associated with small polar caps heated by pulsar-induced return currents striking the magnetic poles (Zavlin 2006). A good example of this is PSR J0437 (Bogdanov et al 2007). Where X-ray pulsations are detected they have been associated with this spectral component as well (Bogdanov 2013). The inferred temperature of this component, ~ 200 eV, tends to be higher than the global surface temperature (Durant et al. 2012), but the emission arises from only a small fraction of the NS surface, consistent with the polar cap interpretation. As we describe below, it is likely that our targets may have such polar cap emission, but it is important to recognize that global temperature constraints can still be derived. These stars have very low magnetic fields $\leq 10^8$ G that do not appreciably distort or beam the atmospheric emission that must be present over their entire surfaces.

2.1. PSR J1640+2224

We selected source counts in a $1.5''$ circular region around the target coordinates. The background is selected from three source-free $9''$ radii regions distributed around the source. The data processing was performed using CIAO 4.8. The left panel of Fig. 2 shows the image of the ACIS-S exposure around PSR J1640+2224. The green circle shows the $1.5''$ region centered on the position of the source (RA: $16^h40^m16.7^s$ Dec: $22^\circ24'8.9''$). In total there are 32 counts in the ~ 40.8 ksec exposure (considering all 1024 detector energy channels). This is a very strong detection for such an exposure, given *Chandra's* superb angular resolution and low background, and represents the first detection of J1640 in the X-ray band. Although the total number of observed source counts is not high enough for a detailed spectral analysis, it is still sufficient to constrain the surface temperature of the star.

The spectral analysis is performed using XSPEC version 12.8.2 (Arnaud 1996). All but two counts in the source extraction region have an energy below 3 keV, which is consistent with the expected, soft X-ray spectrum of other MSPs. Thus, we consider only the 0.1 – 3 keV energy band (ACIS channels 8 – 205) for spectral analysis. The net count rate in the source region is $7.21 \times 10^{-4} \pm 1.34 \times 10^{-4}$ cts/s, with a total of 30 counts. To take into account the effects of interstellar absorption we adopt a galactic absorbing column, n_H , determined

with HEASARC's " n_H -tool," and we use the *wabs* photoelectric absorption model in XSPEC (Morrison & McCammon 1983).

Since the number of counts in each channel is small, in our spectral fitting we use the C-statistic (*cstat* in XSPEC), which is the maximum likelihood-based statistic appropriate for Poisson data (Cash 1979), instead of the χ^2 statistic. We note that in the limit of large numbers of counts this statistic asymptotes to χ^2 . The C-statistic can be used regardless of the number of counts in each bin, and an approximate goodness-of-fit measure for a given value of the *cstat* statistic can be obtained by dividing the observed statistic by the number of degrees of freedom, which should be of the order of 1 for good fits.

To model the spectrum we use the NS hydrogen atmosphere model *nsatmos* in XSPEC (Heinke et al. 2006). We employ this model rather than a blackbody, because during the evolution of MSPs they accrete a substantial amount of matter and it is expected that they have an atmospheric layer on their surfaces. Fitting a blackbody to a MSP spectrum results in a smaller inferred emission area and a higher temperature compared to fitting a hydrogen atmosphere model (Zavlin 2006; Bogdanov 2013). To constrain the global surface temperature of the star we first fit the spectrum with an absorbed hydrogen atmosphere model (*wabs*nsatmos*), fixing the NS mass, radius, and n_H , and find the best values for the other two parameters, namely the temperature and the normalization (defined as the fraction of the NS surface that is emitting, hereafter, norm1). We find that the inferred temperature and emitting area are consistent with the existence of a hotspot on the NS surface. However, in order to constrain the NS's core temperature, we need an upper limit on the global surface temperature of the star, which is expected to be lower than the hotspot temperature. Therefore we fix all the hotspot model parameters to their best-fit values and add another hydrogen atmosphere model component to account for the global surface emission, and fit the spectrum again. The full XSPEC model in this case is *wabs*(nsatmos+nsatmos)*. For the second, surface emission *nsatmos* model, we fix the values of n_H , NS mass, and radius to the same values as for the hotspot component, and we also fix the value of the normalization parameter for this component, norm2, to 1.0-norm1, and in this case norm2 ~ 1 . Then we fit the spectrum again to constrain the value of the second (surface) temperature parameter.

To put an upper limit on the global surface temperature of the star we fix all the model parameters except the second temperature and vary that parameter using the *steppar* command in XSPEC until the C-statistic changes by 2.706, equivalent to the 90% confidence region for a single interesting parameter. The result is shown in the right panel of Fig. 3. We do the same procedure for two different NS models with masses and radii of $1.4 M_\odot$ and 11.5 km, and $2.21 M_\odot$ and 10 km¹. The resulting spectral model parameters for PSR J1640+2224 are given in Table 2.

We tried three different hydrogen atmosphere models (*nsa*, *nsagrav*, and *nsatmos*), and a helium atmosphere

¹ Here, radii are computed using the Akmal-Pandharipande-Ravenhall (APR) equation of state (Akmal et al. 1998).

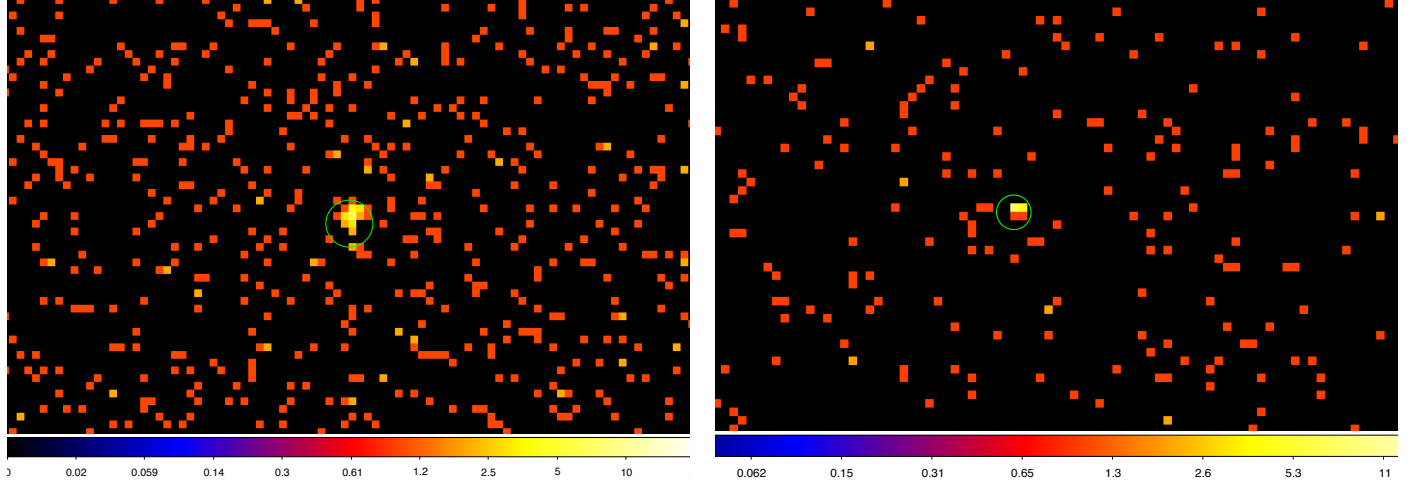


FIG. 2.— Left: The image of the ACIS-S exposure (~ 40794 s) around PSR J1640+2224. The green circle shows the $1.5''$ region centered on the position of the source (RA: $16^h 40^m 16.7^s$ Dec: $22^\circ 24' 8.9''$). Right: merged image of the two ACIS-S exposures (29716 s and 26758 s) around PSR J1709+2313. The green circle shows the $1.5''$ region centered on the position of the source (RA: $17^h 9^m 5.8^s$ Dec: $23^\circ 13' 27.8''$)

TABLE 1
CHANDRA OBSERVATIONS OF PSR J1640+2224 AND PSR J1709+2313

	Obs-ID	Date	Exposure (s)	ν_{spin} (Hz)	$\frac{d\nu}{dt} _{obs}$ (Hz s $^{-1}$)	P_b (days)	d (kpc)	n_H ($\times 10^{22}$ cm $^{-2}$)
PSR J1640+2224	16746	2015 Dec 23	40794	316.12	-1.63×10^{-16}	175.46	1.50	0.044
PSR J1709+2313	16747	2016 Mar 12	26758	215.93	-6.9×10^{-17}	22.71	2.18	0.046
	18801	2016 Mar 10	29716					

NOTE. — *Chandra* observation ID, date of observation, exposure time, spin frequency, observed spin-down rate from pulsar timing, orbital period, distance to the source and hydrogen column density. The spin-down rates and distance values are from the ATNF Pulsar Catalogue (Manchester et al. 2005; Yao et al. 2017)

TABLE 2
CHANDRA ACIS-S BEST SPECTRAL MODELS FOR PSR J1640+2224

Model	M M_\odot	R (km)	norm1	Log $T_{eff,1}$ (K)	norm2	Log $T_{eff,2}$ (K)	Model predicted rate (cts/s)	Cstat/dof
<i>wabs*(nsatmos+nsatmos)</i>	1.4	11.5	1.5×10^{-4}	6.32	1.0	5.41 ± 0.12	7.3×10^{-4}	101.5/197
<i>wabs*(nsatmos+nsatmos)</i>	2.21	10	1.0×10^{-4}	6.46	1.0	5.53 ± 0.12	7.3×10^{-4}	101.4/197

NOTE. — The values of N_H and the distance to the source are fixed at 0.044×10^{22} cm $^{-2}$ and 1.5 kpc, respectively.

model (*nsx*) in XSPEC in our spectral analysis, and for the range of parameters that we are interested they give very similar results. We have chosen to use the *nsatmos* model since it has a separate parameter (“norm,” described above) for the emitting area that makes it easier to work with. With the He atmosphere model, fitting only one component (i.e. *wabs*nsx*) gives a comparable fit to the one-component H atmosphere model (*wabs*nsatmos*), but after adding the second component to the fit to constrain the global surface temperature, it does not give as good a fit as the two *nsatmos* model fits in some cases, since the temperature of the second component in *nsx* cannot go below $\text{Log } T_{eff} = 5.5$.

We also tried fitting both *nsatmos* models at the same time (still keeping the second normalization parameter fixed at 1) and it gave similar results as fitting two components separately. The differences in the values of the

second temperature parameter (global surface temperature) are very small and within the error bar (for example, the difference is less than 1 eV in the case of J1640).

2.2. PSR J1709+2313

The observation of J1709 was done in two parts, for a total exposure of 56.5 ksec (see Table 1 for details). Similarly to J1640 we selected the source counts in a $1.5''$ circular region around the target coordinates and the background from 3 source-free $9''$ radii regions distributed around the source. The green circle in the right panel of Fig. 2 shows the $1.5''$ region centered on the position of the source (RA: $17^h 9^m 5.8^s$ Dec: $23^\circ 13' 27.8''$). After extracting spectra and responses for each observation we used *combine-spectra* in CIAO 4.8 to coadd the spectra and responses. In total there are 13 counts in the 0.1-3 keV band, and the net count rate is $2.19 \times 10^{-4} \pm$

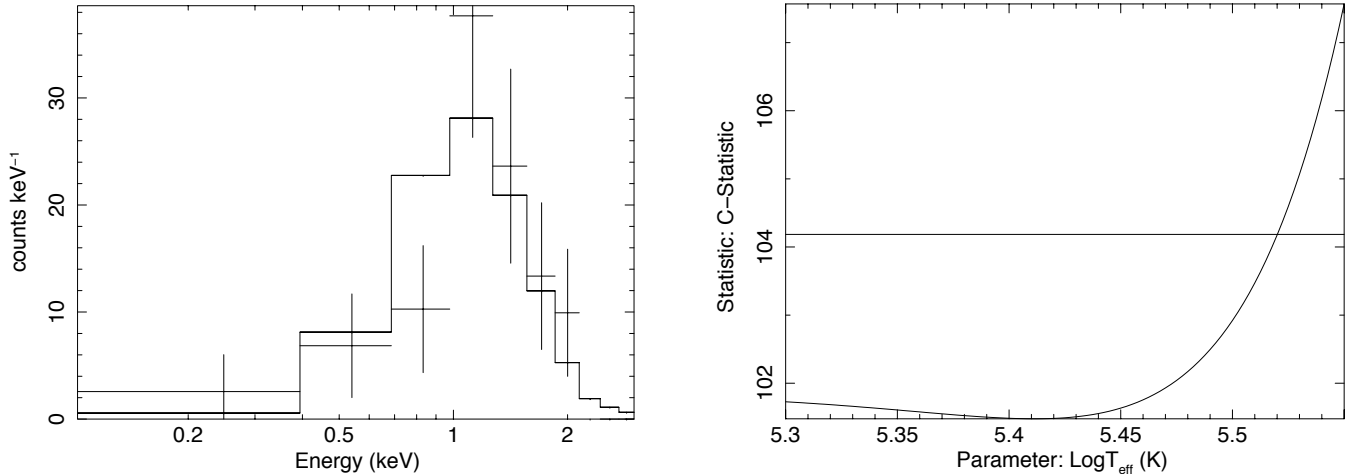


FIG. 3.— Left: Chandra ACIS-S X-ray spectrum and the folded model ($wabs^*(nsatmos+nsatmos)$) for J1640 in the 0.1-3 keV energy band. The NS mass and radius in these models are fixed at $1.4 M_{\odot}$ and 11.5 km, respectively. Right: confidence region for the second temperature parameter in the fit of the two absorbed hydrogen atmosphere models. The horizontal line shows the 90% confidence region.

6.39×10^{-5} cts/s during 56.5 ksec total exposure. There are a few photons above 9 keV that have been ignored in our spectral analysis. We carried out a similar procedure as for J1640 to fit the spectrum with an absorbed hydrogen atmosphere model, $wabs^*(nsatmos+nsatmos)$ in XSPEC. The results of our best fits for two NS models with a canonical and a high-mass are given in Table 3. The left panel of Fig. 4 shows the data and folded model for a $1.4 M_{\odot}$ star, and the right panel shows the upper limit on the global surface temperature, similar to Fig. 3.

3. CONSTRAINING THE R -MODE AMPLITUDE AND SPIN-DOWN RATE

In order to constrain the amplitude of the r -mode oscillations in these pulsars, we first need to compute the core temperatures using the surface temperature limits we obtained from spectral fitting in section 2. We use the following equation that relates the effective surface temperature of the star, T_{eff} , to the internal temperature, T_b , which is the temperature at a fiducial boundary at $\rho_b = 10^{10}$ g cm^{-3} for a fully accreted envelope and is valid for $T_b \leq 10^8$ K (Potekhin et al. 1997),

$$\left(\frac{T_{eff}}{10^6 K}\right)^4 = \left(\frac{g}{10^{14} cm s^{-2}}\right) \left(18.1 \frac{T_b}{10^9 K}\right)^{2.42} \quad (1)$$

where $g = GM/(R^2 \sqrt{1 - r_g/R})$ is the surface gravity and $r_g = 2GM/c^2$. Here we assume that the neutron star's core is isothermal and since the thermal conductivity of the crust is high (Brown & Cumming 2009) we have $T_{core} = T_b$ to good approximation. For a partially accreted envelope the core temperature would be slightly higher, but the difference is negligible for our cases (see equation A9 in Potekhin et al. (1997)). The values of the core temperatures are given in Table 5. Having the core and surface temperatures we can now determine the photon and neutrino luminosities using the following equations (see MS13):

$$L_{\gamma} = 4\pi R^2 \sigma T_{eff}^4 \quad (2)$$

where R and T_{eff} are the stellar radius and surface temperature, respectively, and

$$L_{\nu} = \frac{4\pi R_{DU}^3 \Lambda_{QCD}^3 \tilde{L}_{DU}}{\Lambda_{EW}^4} T^6 + \frac{4\pi R^3 \Lambda_{QCD} \tilde{L}_{MU}}{\Lambda_{EW}^4} T^8 \quad (3)$$

where T is the core temperature, R_{DU} is the radius of the core where direct Urca neutrino emission is allowed, and \tilde{L} is a dimensionless parameter given in Table 4. Λ_{QCD} and Λ_{EW} are characteristic strong and electroweak scales with values of 1 GeV and 100 GeV, respectively, that we have used in our calculations.

Assuming that r -modes are excited in these neutron stars, we can use the thermal equilibrium argument discussed in Brown & Ushomirsky (2000; MS13) to put an upper limit on their r -mode amplitudes. We note that based on their inferred core temperatures, these pulsars lie in the uncertainty region of the r -mode instability window (see Fig. 6 of Schwenzer et al. 2017) and r -mode oscillations might be completely damped in these sources. However, we still compute the upper limits on their r -mode amplitudes assuming that they are within the unstable region.

We consider that an NS to be in thermal equilibrium when the reheating due to r -mode dissipation is balanced by cooling due to core neutrino emission and the thermal photon emission from the surface of the star, $W_d = L_{\nu} + L_{\gamma}$. The reheating due to r -mode dissipation can be computed using the equation $W_d = -2E_c/\tau_{GR}$ (MS13).

Since W_d is a function of r -mode amplitude, α , one can place an upper limit on α assuming that r -mode dissipation is the only source of heat inside the star

$$\alpha = \frac{5 \times 3^4}{2^8 \tilde{J} M R^3 \Omega^4} \left(\frac{L_{\gamma} + L_{\nu}}{2\pi G}\right)^{1/2} \quad (4)$$

Upper limits on α for two different NS models with canonical and high mass are given in Table 5. These bounds are about an order of magnitude lower than the

TABLE 3
CHANDRA ACIS-S BEST SPECTRAL MODELS FOR PSR J1709+2313

Model	M M_{\odot}	R (km)	norm1	Log $T_{eff,1}$ (K)	norm2	Log $T_{eff,2}$ (K)	Model Predicted Rate (cts/s)	Cstat/dof
<i>wabs(nsatmos+nsatmos)</i>	1.4	11.5	3.9×10^{-5}	6.41	1.0	5.50 ± 0.04	2.63×10^{-4}	70.1/197
<i>wabs(nsatmos+nsatmos)</i>	2.21	10	4.2×10^{-5}	6.50	1.0	5.61 ± 0.04	2.57×10^{-4}	70.6/197

NOTE. — The values of n_H and the distance to the source are fixed at $0.046 \times 10^{22} \text{ cm}^{-2}$ and 2.18 kpc, respectively.

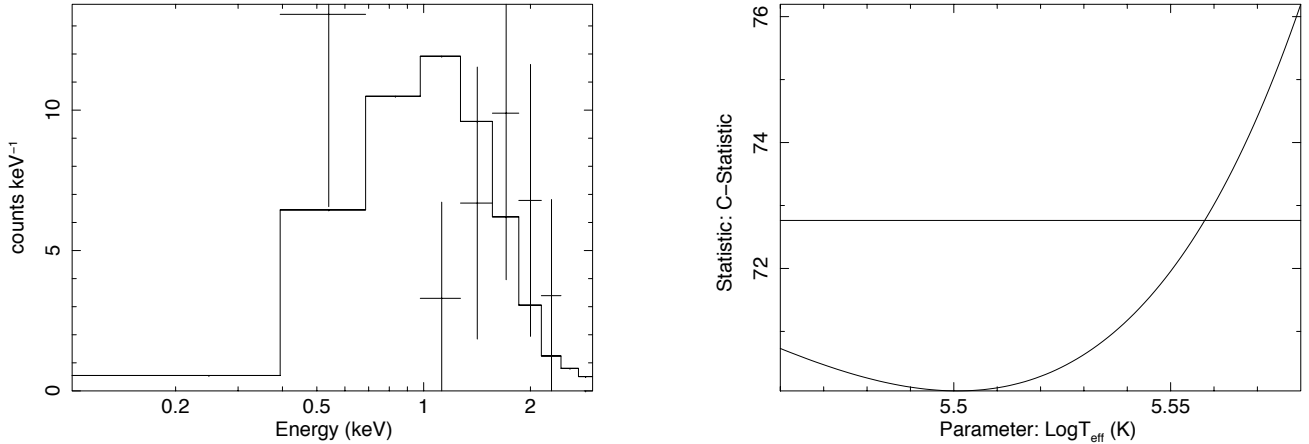


FIG. 4.— Left: Chandra ACIS-S X-ray spectrum and the folded model (*wabs*(nsatmos+nsatmos)*) for J1709 in the 0.1-3 keV energy band. The NS mass and radius in these models are fixed at $1.4 M_{\odot}$ and 11.5 km, respectively. Right: Confidence region for the second temperature parameter in the fit of the two absorbed hydrogen atmosphere models. The horizontal line shows the 90% confidence region.

TABLE 4
PARAMETERS OF THE NEUTRON STAR MODELS

Neutron Star	Shell	$R(km)$	$\Omega_K(Hz)$	\tilde{I}	\tilde{J}	\tilde{L}
NS $1.4 M_{\odot}$	Core	11.5	6020	0.283	1.81×10^{-2}	1.91×10^{-2}
NS $2.21 M_{\odot}$	m.U. core	10.0	9310	0.295	2.02×10^{-2}	1.29×10^{-2}
	d.U. core	5.9				2.31×10^{-5}

NOTE. — Radius, Kepler frequency and radial integral parameters that appear in the moment of inertia, angular momentum of the mode, and neutrino luminosity for different neutron star models considered in this work (Alford et al . 2010, 2012a). For the $2.21 M_{\odot}$ model the neutrino luminosity parameter is different in the inner core where direct Urca processes are allowed, therefore these values are given separately in the last row.

bounds obtained for LMXB sources with comparable frequencies (MS13), because of the lower temperature limits in these pulsars compared to LMXBs.

To obtain limits on r -mode spin-down rates we note that since these neutron stars are old, if they are inside the r -mode instability window, their r -mode amplitudes should be saturated by some mechanism, meaning $\frac{d\alpha}{dt} = 0$, otherwise they would have been spun down long before. This implies that $\frac{1}{\tau_v} = -\frac{1}{\tau_G} \frac{1}{1-\alpha^2 Q}$ in the saturation regime, where $Q = 3\tilde{J}/2\tilde{I}$ (MS13). The values of \tilde{J} and \tilde{I} are given in Table 4. Therefore the equation for the evolution of NS spin frequency can be written as (MS13):

$$\frac{d\Omega}{dt} = 2Q \frac{\Omega \alpha^2}{\tau_G (1 - \alpha^2 Q)} \quad (5)$$

where

$$\frac{1}{\tau_G} = -\frac{P_G}{2E_c} \quad (6)$$

$$E_c = \frac{1}{2} \alpha^2 \Omega^2 \tilde{J} M R^2 \quad (7)$$

$$P_G = \frac{2^{17} \times \pi}{5^2 \times 3^8} \tilde{J}^2 G M^2 R^6 \alpha^2 \Omega^8 \quad (8)$$

E_c is the canonical energy of the r -mode and P_G is the power radiated by gravitational waves. Note that P_G here is given for the $l = m = 2$ r -mode (MS13) which is the most unstable one. The upper limits on the r -mode-induced spin-down rates, along with the observed spin-down rates from pulsar timing for these pulsars, are

TABLE 5
NS TEMPERATURES AND LUMINOSITIES, AND r -MODE AMPLITUDE AND SPIN-DOWN RATES

	ν_{spin} (Hz)	T_{eff} (K)	$g/10^{14}$ (cm/s ²)	T_b (K)	L_γ (erg/s)	L_ν (erg/s)	α	$\frac{d\Omega}{dt} _G$ (Hz/s)	$\frac{d\Omega}{dt} _{obs}$ (Hz/s)
J1640+2224									
1.4M _⊙ , 11.5km	316.12	3.31×10^5	1.755	7.05×10^6	1.13×10^{31}	2.15×10^{22}	3.2×10^{-8}	-1.3×10^{-18}	-1.63×10^{-16}
2.21M _⊙ , 10km		4.28×10^5	4.976	7.01×10^6	2.40×10^{31}	9.18×10^{30}	4.8×10^{-8}	-3.4×10^{-18}	-1.63×10^{-16}
J1709+2313									
1.4M _⊙ , 11.5km	215.93	3.61×10^5	1.755	8.14×10^6	1.61×10^{31}	6.77×10^{22}	1.8×10^{-7}	-2.7×10^{-18}	-6.9×10^{-17}
2.21M _⊙ , 10km		4.68×10^5	4.976	8.12×10^6	3.42×10^{31}	2.21×10^{31}	2.8×10^{-7}	-8.4×10^{-18}	-6.9×10^{-17}

NOTE. — The values of T_{eff} are upper limits on surface temperatures and therefore are slightly higher than the $T_{eff,2}$ given in Tables 2 and 3; g is the surface gravity, T_b is the core temperature, L_γ and L_ν are photon and neutrino luminosities, α is the upper limit on the saturation amplitude of the r -modes, and $\frac{d\Omega}{dt}|_G$ and $\frac{d\Omega}{dt}|_{obs}$ are upper limits on the r -mode-induced spin-down rates and the observed spin-down rates of these pulsars, respectively.

given in Table 5 and shown in Figure 1. Comparing these values we find that for J1640 the r -mode spin-down cannot be more than 2% of the observed spin-down of the pulsar. For J1709 this number is higher, at 12%, but we note that this source might not even have any excited r -mode oscillations in it, since it lies outside but within the uncertainty region of the r -mode instability window for pure hadronic matter.

4. DISCUSSION

We have used *Chandra* ACIS-S observations of J1640 and J1709 in order to constrain their global surface temperatures and put limits on their r -mode amplitudes and corresponding spin-down rates. These observations represent the first detections of these sources in the X-ray band. Unsurprisingly, the objects are faint, with estimated fluxes (0.3 – 3 keV) of 6×10^{-15} and 3×10^{-15} erg cm⁻² s⁻¹ for J1640 and J1709, respectively.

We first fit their *Chandra* spectra with an absorbed hydrogen atmosphere model. The inferred temperatures and emitting areas that we extracted are consistent with the existence of a hotspot on the NS surface. To obtain a limit on the global surface temperature of the star, which is much lower than the hotspot temperature, we add another hydrogen atmosphere model to our fit and fix all the parameters to the best-fit values we obtained initially, except the temperature of the second model. We found upper limits on the global surface temperature of these pulsars that are $\sim 3.3 \times 10^5 - 4.7 \times 10^5$ K, depending on the assumed NS masses and radii. Our results are broadly consistent with the results of Gusakov et al. (2016) where they have given an upper limit of 6×10^5 K for the redshifted surface temperature of MSPs. Note that the values of temperatures given here are the temperatures at the surface of the star, T_s , and not the redshifted ones, T_∞ , where $T_s = (1+z)T_\infty$.

The characteristic spin-down ages of these sources are about 15-16 Gyr (Lorimer 2008), and white dwarf cooling age estimates also indicate that they are at least several gigayears old (Desvignes et al. 2016). In all standard cooling models neutron stars cool to surface temperatures less than 10^4 K in less than 10^7 yr (Page 2009; Yakovlev & Pethick 2004). While we have derived *upper limits* on the surface temperatures for J1640 and J1709, they appear to be consistent with the values *measured*

for J0437 and J2124. Taken together these results suggest that the surface temperatures of at least some MSPs are significantly higher, given their ages, than standard cooling models would suggest.

These high temperatures cannot be attributed to accretion, since the time it takes for the star to cool to such low temperatures (a few million years) is much less than the time since accretion has ceased in the binary system (> 100 Myr) (Willems & Kolb 2002; Kargaltsev et al. 2004). Therefore, some other source of reheating is likely operating in these pulsars. Kargaltsev et al. (2004) and Gonzalez & Reisenegger (2010) have discussed some internal and external sources of heat, which includes: (1) dissipation of the energy of differential rotation caused by frictional interaction between the faster-rotating superfluid core and the slower-rotating solid crust (Shibazaki & Lamb 1989; Larson & Link 1999); (2) energy release due to the cracking of the crust (Cheng et al. 1992) as well as changes in the rate of nuclear reactions due to the readjustment of the NS structure to a new equilibrium state as the star spins down (rotochemical heating; Reisenegger 1995); (3) the energy release due to the pinning and unpinning of the vortex lines with respect to the nuclei of the crystal lattice as the star spins down (vortex creep; Alpar et al. 1984); and (4) magnetospheric heating (Harding & Muslimov 2002). In the case of pulsars that are hot enough to be inside the r -mode instability window, e.g. J1640, then r -mode dissipation can provide another source of reheating.

We used the upper limits on the surface temperature of these pulsars to first calculate their core temperatures, and then the upper limits on their r -mode amplitudes and their r -mode-induced spin-down rates. The limits on the amplitudes are $\sim (3.2 - 4.8) \times 10^{-8}$ and $\sim (1.7 - 2.8) \times 10^{-7}$ for J1640 and J1709, respectively, depending on the assumed NS mass and radius and the existence of fast neutrino cooling in the core. These values are about an order of magnitude lower than the upper bounds obtained for most of the LMXB sources with comparable frequencies (MS13), because of the lower temperatures in these pulsars. Interestingly, the limits for J1640 and J1709 are in line with the upper limits derived for the AMXP SAX J1808.4–3658, which unlike J1640 and J1709, has had recent accretion. The upper bounds on the r -mode spin-down rate for J1640 is

$\sim (1.3-3.4) \times 10^{-18}$ and for J1709 is $\sim (2.7-8.3) \times 10^{-18}$. Comparing these values we find that for J1640 the r -mode spin-down cannot be more than 2% of the observed spin-down of the pulsar, and for J1709 it cannot be more than 12%. As noted previously, both of these systems reside near the boundary of the r -mode instability window and within the uncertainty region, therefore both of them might be r -mode stable, in which case no particularly new physics, either for damping or saturation of the r -mode, would be required to explain such low upper limits.

Here we assumed that these systems are inside the r -mode instability window but their r -modes are saturated at some small amplitudes and are no longer growing. As the star spins down and cools, eventually it will leave the unstable region, but if the saturation amplitude is very small, as is the case for these systems, it can live inside the instability window for a very long time (see Fig. 1 and 2 in Alford et al. 2012c). It doesn't seem unlikely to find two systems in this phase of their evolution, because based on their observed spin-down rates (1.63×10^{-16} Hz/s for J1640 and 6.9×10^{-17} Hz/s for J1709) it would take billions of years to spin down these pulsars by a few Hertz, therefore accretion seems to be the main mechanism that places these systems in their current location in or near the instability window. Given the limits on the temperatures and r -mode saturation amplitudes in these systems, the r -mode-induced spin-down rate can be only a few percent of the observed spin-down rate and it will not have a big effect on their evolution.

It remains an open question whether r -modes are excited with these tiny amplitudes in MSPs or if they are completely damped. Although such low-amplitude r -modes will not have much of an effect on the spin evolution of old pulsars, their dissipation can still provide an extra source of heat for the NS. Then the question would be which mechanism would be able to dampen the r -modes to such low amplitudes. There are several mechanisms that have been proposed (see the introduction for a brief summary), but of these none have been shown to eliminate the r -mode instability or saturate r -mode amplitudes at such low values. One process that could perhaps saturate r -mode amplitudes at very low levels is phase conversion in a multicomponent compact star (Alford et al. 2015), which can saturate r -modes at amplitudes smaller than 10^{-10} ; however, that also depends on the microscopic and astrophysical parameters of the star, such as the mass of the quark core, which should not be too small. Dissipation of r -modes at such low amplitudes in hybrid stars will not provide enough heating to affect the temperature of the star. Another interesting proposal for suppression of the r -mode instability at certain stellar temperatures is resonant mode coupling and enhanced damping of r -modes in NSs with a superfluid core (Gusakov et al. 2014; Kantor et al. 2016).

Looking ahead, measurements or upper bounds on the surface temperature of MSPs, especially those with higher spin frequencies, which are expected to be inside the nominal instability window for hadronic matter, will provide a valuable tool to study r -mode physics and constrain the properties of neutron star interiors. MSPs with $T_{eff}^{\infty} > 6 \times 10^5$ K would provide strong evidence

for the existence of unstable r -modes in such pulsars (Gusakov et al. 2016), since r -mode dissipation would be the most natural source of heating in the absence of accretion.

Support for this work was provided by the National Aeronautics and Space Administration through Chandra Award Number GO5-16049Z issued by the Chandra X-ray Observatory Center, which is operated by the Smithsonian Astrophysical Observatory for and on behalf of the National Aeronautics Space Administration under contract NAS8-03060. S.M.'s research was supported by an appointment to the NASA Postdoctoral Program at the GSFC.

REFERENCES

- Akmal, A., Pandharipande, V. R., & Ravenhall, D. G. 1998, Phys. Rev. C, 58, 1804
- Alford, M. G., Han, S., & Schwenzer, K. 2015, Phys. Rev. C, 91, 055804
- Alford, M. G., Mahmoodifar, S., & Schwenzer, K. 2010, Journal of Physics G Nuclear Physics, 37, 125202
- Alford, M. G., Mahmoodifar, S., & Schwenzer, K. 2012a, PhRvD, 85, 024007
- Alford, M. G., Mahmoodifar, S., & Schwenzer, K. 2012b, Phys. Rev. D, 85, 044051
- Alford, M. G., Mahmoodifar, S., & Schwenzer, K. 2012c, in AIP Conf. Proc. 1492, QCD@WORK 2012: International Workshop on Quantum Chromodynamics: Theory and Experiment, ed. L. Angelini, G. E. Bruno, G. Chioldini et al. (Melville, NY: AIP), 257
- Alford, M. G., & Schwenzer, K. 2013, arXiv:1310.3524
- Alpar, M. A., Pines, D., Anderson, P. W., & Shaham, J. 1984, ApJ, 276, 325
- Andersson, N., Kokkotas, K. D., & Stergioulas, N. 1999, ApJ, 516, 307
- Arras, P., Flanagan, E. E., Morsink, S. M., et al. 2003, ApJ, 591, 1129
- Arnaud, K. A. 1996, in ASP Conf. Ser. 101, Astronomical Data Analysis Software and Systems V, ed. G. H. Jacoby & J. Barnes (San Francisco, CA: ASP), 17
- Bildsten, L. 1998, ApJL, 501, L89
- Bildsten, L., & Ushomirsky, G. 2000, ApJ, 529, L33
- Bogdanov, S., Rybicki, G. B., & Grindlay, J. E. 2007, ApJ, 670, 668
- Bogdanov, S. 2013, ApJ, 762, 96
- Bondaescu, R., Teukolsky, S. A., & Wasserman, I. 2007, Phys. Rev. D, 76, 064019
- Bondaescu, R., Teukolsky, S. A., & Wasserman, I. 2009, Phys. Rev. D, 79, 104003
- Brown, E. F., & Cumming, A. 2009, ApJ, 698, 1020
- Brown, E. F., & Ushomirsky, G. 2000, ApJ, 536, 915
- Cash, W. 1979, ApJ, 228, 939
- Chakrabarty, D., Morgan, E. H., Munro, M. P., et al. 2003, Natur, 424, 42
- Cheng, K. S., Chau, W. Y., Zhang, J. L., & Chau, H. F. 1992, ApJ, 396, 135
- Desvignes, G., Caballero, R. N., Lentati, L., et al. 2016, MNRAS, 458, 3341
- Durant, M., Kargaltsev, O., Pavlov, G. G., et al. 2012, ApJ, 746, 6
- Gonzalez, D., & Reisenegger, A. 2010, A&A, 522, A16
- Gusakov, M. E., Chugunov, A. I., & Kantor, E. M. 2014, Physical Review Letters, 112, 151101
- Gusakov, M. E., Chugunov, A. I., & Kantor, E. M. 2016, arXiv:1610.06380
- Harding, A. K., & Muslimov, A. G. 2002, ApJ, 568, 862
- Haskell, B., & Andersson, N. 2010, MNRAS, 408, 1897
- Haskell, B., Andersson, N., & Passamonti, A. 2009, MNRAS, 397, 1464
- Haskell, B., Degenaar, N., & Ho, W. C. G. 2012, MNRAS, 424, 93
- Haskell, B., Glampedakis, K., & Andersson, N. 2014, MNRAS, 441, 1662
- Heinke, C. O., Rybicki, G. B., Narayan, R., & Grindlay, J. E. 2006, ApJ, 644, 1090
- Ho, W. C. G., Andersson, N., & Haskell, B. 2011, PhRvL, 107, 101101
- Kantor, E. M., Gusakov, M. E., & Chugunov, A. I. 2016, MNRAS, 455, 739
- Kargaltsev, O., Pavlov, G. G., & Romani, R. W. 2004, ApJ, 602, 327
- Larson, M. B., & Link, B. 1999, ApJ, 521, 271
- Levin, Y., & Ushomirsky, G. 2001, MNRAS, 324, 917
- Löhmer, O., Lewandowski, W., Wolszczan, A., & Wielebinski, R. 2005, ApJ, 621, 388
- Lorimer, D. R. 2008, Living Reviews in Relativity, 11, 8
- Lundgren, S. C., Foster, R. S., & Camilo, F. 1996, in ASP Conf. Ser. 105, IAU Coll. 160, Pulsars: Problems and Progress, ed. S. John-

- ston, M. A. Walker, & M. Bailes (San Francisco, CA: ASP), 497
- Mahmoodifar, S., & Strohmayer, T. 2013, *ApJ*, 773, 140
- Manchester, R. N., Hobbs, G. B., Teoh, A., & Hobbs, M. 2005, *AJ*, 129, 1993
- Morrison, R., & McCammon, D. 1983, *ApJ*, 270, 119
- Page, D. 2009, *Astrophysics and Space Science Library*, 357, 247
- Patruno, A. 2010, *ApJ*, 722, 909
- Patruno, A., & Watts, A. L. 2012, arXiv:1206.2727
- Potekhin, A. Y., Chabrier, G., & Yakovlev, D. G. 1997, *A&A*, 323, 415
- Rangelov, B., Pavlov, G. G., Kargaltsev, O., et al. 2017, *ApJ*, 835, 264
- Reisenegger, A. 1995, *ApJ*, 442, 749
- Rezzolla, L., Lamb, F. K., Marković, D., & Shapiro, S. L. 2001, *Phys. Rev. D*, 64, 104014
- Rezzolla, L., Lamb, F. K., & Shapiro, S. L. 2000, *ApJ*, 531, L139
- Schwenzer, K., Boztepe, T., Güver, T., & Vurgun, E. 2017, *MNRAS*, 466, 2560
- Shibazaki, N., & Lamb, F. K. 1989, *ApJ*, 346, 808
- White, N. E., & Zhang, W. 1997, *ApJL*, 490, L87
- Willems, B., & Kolb, U. 2002, *MNRAS*, 337, 1004
- Yakovlev, D. G., & Pethick, C. J. 2004, *ARA&A*, 42, 169
- Yao, J. M., Manchester, R. N., & Wang, N. 2017, *ApJ*, 835, 29
- Zavlin, V. E. 2006, *ApJ*, 638, 951